Adsorption of Frog Foam Nest Proteins at the Air-Water Interface

Alan Cooper,* Malcolm W. Kennedy,† Rachel I. Fleming,*† Emma H. Wilson,*† Hortense Videler,*† David L. Wokosin,‡ Tsueu-ju Su,§ Rebecca J. Green,§ and Jian R. Lu§

*Department of Chemistry and †Institute of Biomedical and Life Sciences, University of Glasgow, Glasgow, United Kingdom; ‡Centre for Biophotonics, Strathclyde Institute for Biomedical Sciences, University of Strathclyde, Glasgow, United Kingdom; and §Biological Physics Group, University of Manchester, Manchester, United Kingdom

ABSTRACT The surfactant properties of aqueous protein mixtures (ranaspumins) from the foam nests of the tropical frog *Physalaemus pustulosus* have been investigated by surface tension, two-photon excitation fluorescence microscopy, specular neutron reflection, and related biophysical techniques. Ranaspumins lower the surface tension of water more rapidly and more effectively than standard globular proteins under similar conditions. Two-photon excitation fluorescence microscopy of nest foams treated with fluorescent marker (anilinonaphthalene sulfonic acid) shows partitioning of hydrophobic proteins into the air-water interface and allows imaging of the foam structure. The surface excess of the adsorbed protein layers, determined from measurements of neutron reflection from the surface of water utilizing H_2O/D_2O mixtures, shows a persistent increase of surface excess and layer thickness with bulk concentration. At the highest concentration studied (0.5 mg ml^{-1}), the adsorbed layer is characterized by three distinct regions: a protruding top layer of ~20 Å, a middle layer of ~30 Å, and a more diffuse submerged layer projecting some 25 Å into bulk solution. This suggests a model involving self-assembly of protein aggregates at the air-water interface in which initial foam formation is facilitated by specific surfactant proteins in the mixture, further stabilized by subsequent aggregation and cross-linking into a multilayer surface complex.

INTRODUCTION

Foam nesting is one of numerous strategies evolved in tropical frogs to protect their eggs and develop tadpoles against environmental challenges. *Physalaemus pustulosus*—the common mud puddle ''túngara'' frog of Central/South America and parts of the Caribbean—produces voluminous protein foam nests containing fertilized eggs. These foam nests are stable for several days under exposed tropical conditions, and protect the developing embryos and juveniles against dehydration, predation, and microbial degradation, also acting as mini-incubators to facilitate rapid development of eggs and tadpoles (Downie, 1988, 1990, 1993; and Supplementary Material). The unusual stability of these biofoams, together with other properties of the biomaterials used in the nests, has prompted this investigation into some of the factors responsible for such behavior. We report here on our initial biophysical characterization of this material.

P. pustulosus protein foam nests are constructed during mating from a proteinaceous fluid excreted by the female and whipped up by the male, using his legs in a rapid ''egg-beater''-like motion (see Supplementary Material for a video clip). This normally occurs overnight during the rainy season at the edges of temporary standing water, and the nests are subsequently left to fend for themselves, attached to surrounding soil or vegetation. Unlike conventional detergents, which would damage sensitive biological tissues, the components of these foams must be compatible with eggs, sperm, and developing embryos. They must also have appropriate biophysical properties for aqueous foam formation and stabilization. Foaming of proteins is usually best avoided under normal circumstances because of the severe disruptive processes thought to occur at the air-water interface that might lead to denaturation or chemical degradation (Clarkson et al., 1999). Consequently the evolution of proteins specifically adapted for foam formation and stabilization poses interesting questions about their structure and stability. Moreover, the long-term stability and biocompatibility of these protein foams, together with the possible self-assembly of surface structures in these systems, suggests a number of potential biomedical and other technological applications. We have shown elsewhere that the naturally occurring nest foam of *P. pustulosus* contains a mixture of proteins (''ranaspumins''), predominantly in the 10–40 kDa mass range, and have cloned and sequenced cDNAs encoding several of these proteins (R. I. Fleming, A. Cooper, and M. W. Kennedy, unpublished data). All of these sequences are previously unreported in any organism, and translations to amino acid sequences provided only remote matches in current databases. This presents us with the exciting challenge of identifying the function(s) of these proteins in the foam and the structural basis for their activity. This is particularly challenging because, at least for surfactant properties, it is the behavior at the interface (rather than bulk solution) that matters. Here we describe experiments using a range of methods to probe the biophysical properties of the proteins in the bulk phase and the aggregation or assembly of ranaspumins in the natural mixture at the air-water interface. We have used classic surface tension methods to determine the kinetics and

Submitted May 28, 2004, and accepted for publication December 21, 2004.

Address reprint requests to Professor Alan Cooper, Chemistry Department, Glasgow University, Glasgow G12 8QQ, Scotland, UK. E-mail: alanc@chem.gla.ac.uk.

0006-3495/05/03/2114/12 $2.00

doi: 10.1529/biophysj.104.046268

concentration dependence of surfactant properties compared to known proteins. Two-photon excitation fluorescence microscopy and specular neutron reflection (NR) demonstrate the partitioning of proteins into the air-water interface, allowing estimates to be made of the dimensions of the surface assemblies.

MATERIALS AND METHODS

Proteins and reagents

Frog foam nests were collected in the field (Trinidad, Northern Range) during the rainy season (July and August) with proper regard to ecological concerns and with the permission of the Trinidad Wildlife Service. *P. pustulosus* frogs are widespread, common, and not currently an endangered species. We collected only from sites where nests are otherwise usually destroyed by traffic or other human activity. Occasional nests from captive breeding pairs in the lab were also used. Manual separation of foam material (to remove the eggs) was done on site, using laboratory facilities made available to us in the Dept. of Zoology, University of the West Indies, St. Augustine, and materials were stored frozen for return to the United Kingdom. Foam fluid, containing a natural mixture of ranaspumins, was obtained by drainage, gentle centrifugation, or sonication, and either used immediately or lyophilized and refrigerated until use, without any detectable effects on subsequent measurements. Total protein concentrations were determined by conventional ''Bradford assay''/Coomassie blue methods (Bradford, 1976), using bovine serum albumin (BSA) as standard. Total carbohydrate concentrations were determined using the phenol/sulfuric acid method (Dubois et al., 1956) calibrated with glucose. Reference proteins (BSA, hen egg-white lysozyme), ANS (1-anilinonaphthalene-8-sulfonic acid), thioflavin-T, Congo red, and other reagents were obtained from Sigma (Poole, Dorset, UK) unless otherwise indicated. Ultraviolet (UV)/vis absorbances were measured in 1-cm pathlength quartz cuvettes using a Shimadzu (Tokyo, Japan) UV-160A spectrophotometer.

Surface tension

Surface tension was measured both manually (torsion balance) or with a Kruss (Hamburg, Germany) K10 digital tensiometer using the Du Nouy ring method, calibrated using ultrapure water (UHQ, Elga, Wycombe, UK). The platinum ring was cleaned between each reading by rinsing with UHQ water and flaming (Bunsen burner) to remove residual deposits. The freeze-dried protein was dissolved in UHQ water and the reconstituted solution pH was found to be between 6 and 6.5. All the experiments were done at room temperature (23–26°C), and similar results were obtained using fresh foam fluid and reconstituted solutions. Wetting activity was observed by placing 50-μl drops on horizontal hydrophobic surfaces (Nescofilm or Teflon tape), imaged side-on with a digital camera.

Spectroscopy and imaging

Fluorescence emission spectra for ANS/protein mixtures were obtained at room temperature using a Spex Fluoromax II (Spex, Edison, NJ) instrument with 390 nm excitation (λ_{exc}) and 5-nm slits. Liquid samples were observed using standard 1-cm quartz fluorescence cuvettes, whereas intact foam samples were suspended in the excitation beam on the end of a thin rod. For liquid samples the ANS concentration was 10–20 μM, with ~0.1 mg ml^{-1} added protein. Fluorescence labeling of foam samples was achieved by addition of a small volume of dilute ANS solution to a portion of foam, mixing gently to avoid disruption of foam structure. Similar procedures were adopted for Thioflavin T studies, with 10–50 μM dye and $\lambda_{exc} = 365$ or 450 nm, and for intrinsic tryptophan fluorescence ($\lambda_{exc} = 290$ nm) of protein in the absence of dye. Two-photon excitation fluorescence (Zipfel et al., 2003) volume images of foam samples were obtained with a Bio-Rad Radiance 2000MP laser-scanning system (Bio-Rad, Hercules, CA) described in detail elsewhere (Dixon et al., 2001; Wokosin et al., 2004). The images were acquired with a Coherent Vitesse-XT laser (Coherent, Santa Clara, CA) using 810 nm excitation, ~300-fs sample pulse duration (sech^2 pulse shape), and 80 MHz repetition frequency. A Nikon (Tokyo, Japan) CFi-60 plan apo 20x/0.75 air-immersion objective lens was used with image pixels of 2.7 μm, 2.6 μs dwell time, and emission collection from 440 to 500 nm. For the image volume, 30 planar images were acquired with 3-μm steps. CD spectra were recorded at 20°C in a Jasco (Tokyo, Japan) J-600 spectropolarimeter using 0.1-mm pathlength quartz cells.

Neutron reflection

NR experiments were done at the SURF reflectometer (Rutherford Appleton Laboratory, ISIS, Didcot, UK) following established techniques (Lu and Thomas, 1998; Lu et al., 1998, 2000, 2003; Green et al., 2000) using a white beam source with neutron wavelengths in the range 0.5–6.5 Å. The collimated parallel neutron beam was reflected at the air-liquid interface at three different glancing angles of incidence (1.5°, 0.8°, and 0.5°), and the complete reflectivity curves were merged manually. The beam intensity was calibrated with respect to pure D_2O. A flat background was determined by extrapolation to high values of momentum transfer, κ ($\kappa = (4\pi \sin\theta)/\lambda$, where λ is the wavelength and θ is the glancing angle of incidence). Samples were prepared by dissolving lyophilized ranaspumin mixtures in 11:1 H_2O/D_2O to make null reflecting water (NRW) solution, or in D_2O directly. The positive meniscus of the protein solution was created by pouring the solution into a Teflon trough, as in previous work on protein adsorption (Lu and Thomas, 1998; Lu et al., 1998, 2000, 2003; Green et al., 2000), with the troughs mounted onto an antivibration table.

NR data were analyzed using procedures described in detail elsewhere (Lu et al., 1998, 2000) to determine the surface packing of material at the air-water interface. Such methods, as briefly outlined here, can estimate the thickness and volume fractions of protein layers with depth resolution of order 1–3 Å along an axis normal to the plane of the interface.

The principal relationship between neutron reflectivity, $R(\kappa)$, and the chemical composition of the interface are defined in the following three equations:

$$R(\kappa) = (16\pi^2/\kappa^2)|\rho^*(\kappa)|^2; \quad (1)$$

$$\rho^*(\kappa) = \int \exp(-i\kappa z)\rho(z)\,dz; \quad (2)$$

and

$$\rho(z) = \Sigma n_i b_i, \quad (3)$$

where $\rho(z)$ is the scattering length density along the surface normal (z-direction) and n_i is the number density of ith element with scattering density b_i. Since different isotopes have different b_i values, by the use of isotopic substitution a variety of neutron reflection profiles can be produced for a given chemical structure. A particularly useful contrast is obtained using an H_2O/D_2O mixture containing 8 vol % D_2O (NRW) which has zero scattering length density. When a protein is adsorbed at the air-NRW interface, the specular signal is only from the adsorbed protein layer. Such measurements allow the surface excess (the amount of protein adsorbed) to be determined in the absence of signal from the underlying solvent. Alternatively, when the neutron measurements in D_2O are made, information about the extent of immersion of the protein layer into water can be reliably determined. A further advantage of D_2O measurements is that if the adsorbed layer contains a diffuse tail projecting into the bulk solution, the presence of D_2O helps to highlight the distribution of any diffuse region.

The volume fraction of each component in a uniform layer is expressed as

$$\rho = \phi_p\rho_p + \phi_w\rho_w, \quad (4)$$

where ρ_p and ρ_w are the scattering length densities of protein and water and ϕ_p and ϕ_w are the respective volume fractions. Since $\rho_w = 0$ for NRW, this equation can be simplified to remove the water factor, leaving an equation with only the protein term. The surface excess (Γ) is then calculated by

$$\Gamma = M_w\rho\tau/(6.02\times\Sigma m_p b_p) = \rho\tau p/(6.02\,\rho_p), \qquad (5)$$

where M_w is protein's molecular mass, $\Sigma m_p b_p$ is the total scattering length for protein, p is the density of protein in g cm^{-3}, τ is the layer thickness, and ρ_p is the scattering length density of protein in NRW (see Table 1). If τ and $\Sigma m_p b_p$ are in units of Å, ρ in Å^{-2} and M_w in g mol^{-1} then Γ is in units of mg m^{-2}. Although Eqs. 4 and 5 have been developed under the condition of uniform layer distribution, they are directly applicable to each of the sublayers when more than one layer is required to model the density distribution profiles. The total adsorbed amounts are obtained by summing over the sublayers used in the fitting procedure.

Experimental neutron reflectivity profiles were analyzed by means of the optical matrix modelling formalism in which the calculated reflectivity of an assumed layer model was compared with the measured data. The structural parameters were then varied in a least-squares iteration until a best fit was found. The structural parameters used in the fitting were the number of layers, thickness (τ), and the corresponding scattering length density (ρ) for each layer (related to layer composition as in Eq. 3). The choice of the number of sublayers in the model is dependent upon the extent of inhomogeneity across the interface. Up to three layers were required to fit the data adequately here.

RESULTS AND DISCUSSION

P. pustulosus nest foams are mechanically very stable. They resist both mechanical compression and extension, and do not shear easily, yet are sufficiently elastic to conform to different shapes. When observed under low magnification, the material shows the classic wet-foam/dry-foam (''kugelschaum/polyederschaum'') structures characteristic of foams in general (Adamson and Gast, 1997; Weaire and Hutzler, 1999). Depending on age, extent of drainage, and location within the nest, the polyhedral cell structure generally predominates. The overall density of the foam is ~0.1 g cm^{-3}, so ~90% of the structure is air, with the fluid phase made up mainly of endogenous water and frog secretions. Initial biochemical characterization shows that the foam fluid (obtained by drainage, centrifugation, or sonication) contains 1–2 mg ml^{-1} total protein, depending on sample, and a similar quantity of carbohydrate. Preliminary analysis of the foam O-glycans (Simon Parry, Jaspinder Bhandal, Stuart Haslam and Anne Dell, Imperial College, personal communication, 2003) has revealed the presence of both core-1 and core-2 species, with both fucosylation and sialylation. Analysis of the N-glycans has shown both truncated and complex-type glycans, with the majority having a fucosylated core. There is no detectable fat or lipid (<0.01 mg ml^{-1}, using standard extraction/thin layer chromatography techniques), lower than the levels one might anticipate for traditional surfactant activity. Consequently we conclude that the foam formation and stabilization is dominated by the protein and carbohydrate components in the mixture. This is perhaps not unexpected given the biological context, since conventional small-molecule lipids/detergents would be severely disruptive of the sensitive biological tissues (eggs, sperm, tadpoles) that the nests are intended to protect.

TABLE 1 Structural parameters for a single-layer model obtained from measurements in NRW*

Concentration/ mg ml^{-1}	τ/Å	$\rho \times 10^6$/Å^{-2}	$\Gamma \pm 0.3$/mg m^{-2}	$\phi_p \pm 0.05$
0.001	13 ± 3	0.6 ± 0.2	0.54	0.3
0.007	40 ± 5	0.6 ± 0.1	1.65	0.3
0.05	70 ± 5	0.6 ± 0.1	2.9	0.3
0.5	75 ± 10	0.8 ± 0.1	4.2	0.4

Parameters were calculated using the average scattering length densities estimated for standard proteins, $\rho_{NRW} = 2.03 \times 10^{-6}$ Å^{-2} and $\rho_{D_2O} = 3.28 \times 10^{-6}$ Å^{-2}.

Although superficially similar to the beating of egg white for cooking, production of frog nest foam requires much lower protein concentrations. Total protein concentrations in (hen) egg white (comprising mainly ovalbumin and ovomucoid) usually exceed 90 mg ml^{-1} (Powrie, 1973), compared to the ~1 mg ml^{-1} seen here (or even less, before drainage, when diluted with pond water during the nesting process). Furthermore, egg white and other mucus-like biofoams are also considerably more viscous than foam fluid, allowing entrapment of air during beating in a way that is not feasible with less viscous fluids. Foaming is, nonetheless, often observed with more dilute protein solutions, especially when chemical modification or partial unfolding of the protein is involved (see, e.g., van Koningsveld et al., 2002), and is best avoided during normal protein chemistry activities, but the resulting foams lack the long-term stability of the natural protein foams described here. By contrast, frog nest foams collected in the field are very stable and, in the absence of eggs or tadpoles, remain intact and show little evidence of collapse or dehydration for many days (~10) under ambient tropical conditions. Foams regenerated in the laboratory from foam fluids or nests dispersed in water (using whipping methods similar to those described in van Koningsveld et al., 2002) are similarly stable.

The foam is consequently difficult to handle, and protein separation by conventional chromatographic methods is only partially successful. Sodium dodecyl sulfate (SDS) polyacrylamide gel electrophoresis shows a number of proteins in the 10–40 kDa range, none of them detectably glycosylated, with some additional bands at higher molecular sizes. Control experiments show that these proteins do not come from disrupted eggs. Diluted foam fluid shows intrinsic fluorescence typical of folded globular proteins (Fig. 1 *a*) with $\lambda_{em} = 336$ nm, characteristic of buried tryptophan side chains. Circular dichroism (CD) spectra of the protein mix suggest predominantly β-sheet secondary structure (Fig. 1 *b*). Analysis using standard protein CD algorithms (Provencher and Glöckner, 1981; Sreerama and Woody, 1993) gives the following average secondary structure content: 8.5% α-helix, 42.7% antiparallel β-sheet, 2.7% parallel β-sheet, 19.7% β-turn, and 23.4% other.

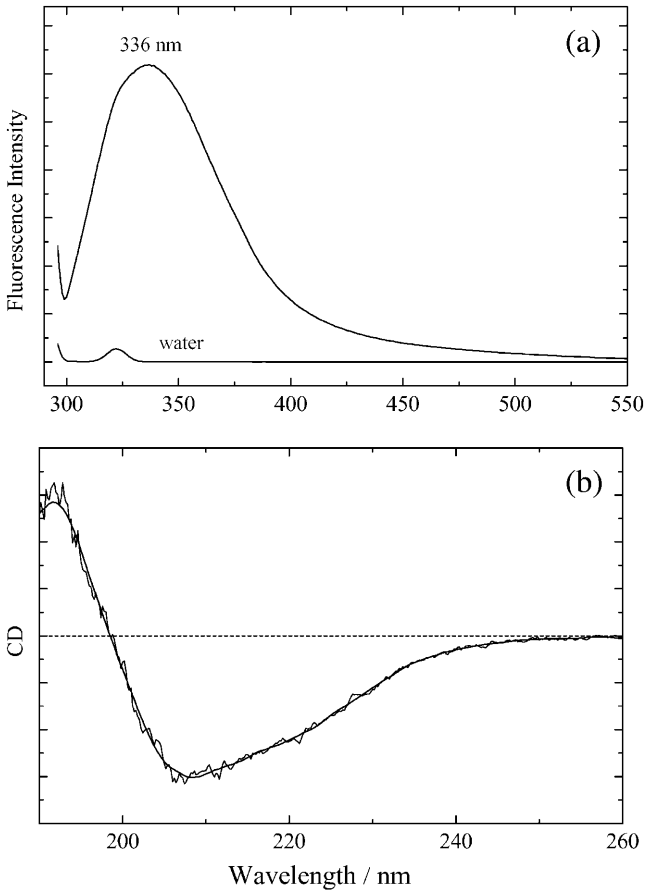

FIGURE 1 (*a*) Fluorescence emission spectrum of diluted foam fluid (0.1 mg ml^{-1} protein) in water (λ_{exc} = 290 nm) with emission maximum (λ_{em}) ~336 nm, characteristic of tryptophan side chains in a nonpolar environment. Water baseline shown for comparison. (*b*) Far-UV circular dichroism (arbitrary units, raw data, and smoothed fit) spectrum of foam fluid (0.5 mg ml^{-1} protein, 0.1-mm pathlength), typical of a protein mixture containing predominantly β-secondary structure.

Surface tension

The natural frog foam mixture extracted from nests of *P. pustulosus* shows strong surfactant properties and is particularly effective in wetting hydrophobic surfaces and reducing the surface tension of water (Fig. 2). At total protein concentrations above ~1 μg ml^{-1} the surface tension drops sharply from the pure water value (~74 mN m^{-1}), falling to ~50 mN m^{-1} at the higher concentrations present in the natural foam (~1 mg ml^{-1}). Although this does not quite match the remarkable surfactant and wetting behavior of the fungal hydrophobins (van der Vegt et al., 1996; Wösten and de Vocht, 2000; Hakanpää et al., 2004), it does contrast markedly with the behavior of common globular proteins such as lysozyme (nonsurfactant under these conditions) or BSA (Fig. 2). The latter is known to have mild surfactant activity, possibly due to indigenous fatty acid content, but is less effective on a w/w basis in comparison here with the frog foam mixture. Other proteins such as the caseins or

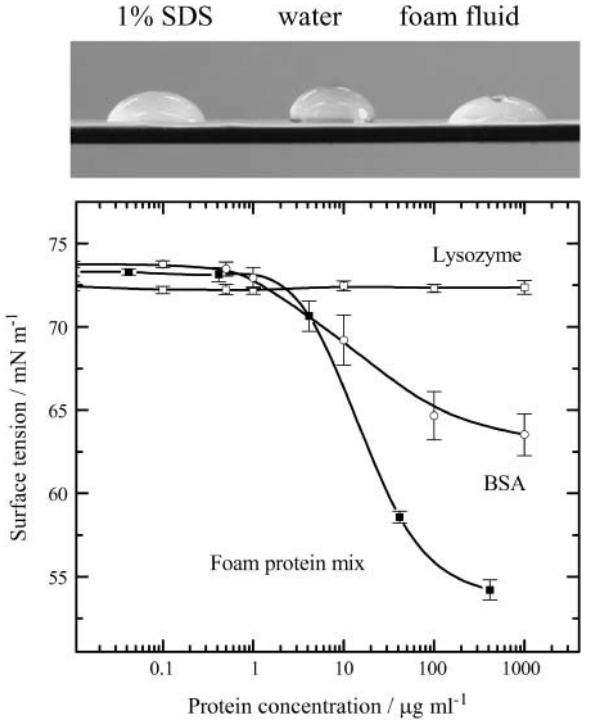

FIGURE 2 Comparison of surfactant properties of dilute frog foam proteins. (*Upper panel*) Side-on images illustrating the wetting of a hydrophobic surface (Nescofilm) by 50-μl drops of foam nest fluid, compared to water, and 1% w/v sodium dodecyl sulfate (SDS) solution. (*Lower panel*) Surface-tension data for serial dilutions of frog foam fluid in water, compared to lysozyme (in acetate buffer, pH 4.5) and BSA (in phosphate buffer, pH 7). (Note: the small differences in surface tension at very low concentrations reflect the different buffers used for each sample. Lysozyme was measured in acidic buffer to avoid the aggregation known to occur with this protein at neutral pH and above.)

β-lactoglobulins can exhibit similar surface tension effects, though these proteins are not presumably evolved for this purpose and their surfactant activities often involve denaturation or chemical modification (Mackie et al., 1999; McClellan and Franses, 2003). The surfactant activity of the frog foam fluid is even more remarkable when one bears in mind that the natural fluid extracted from nests comprises a mixture of proteins with possibly different functions, presumably not all of them contributing to the surface tension properties (R. I. Fleming, A. Cooper, and M. W. Kennedy, unpublished data). This reduction in surface tension is also manifest in the significant wetting ability and reduction in contact angle of small drops placed on hydrophobic surfaces (Fig. 2), comparable to effects seen with much smaller molecules such as SDS.

A characteristic feature of protein surface adsorption previously observed with known proteins is the variation of surface tension with time (du Noüy, 1922a,b; Graham and Phillips, 1979; Damodaran and Song, 1988; Song and Damodaran, 1991; Anand and Damodaran, 1995), and we observed similar behavior with the frog foam mixture (Fig. 3). The initial drop in surface tension in the freshly formed

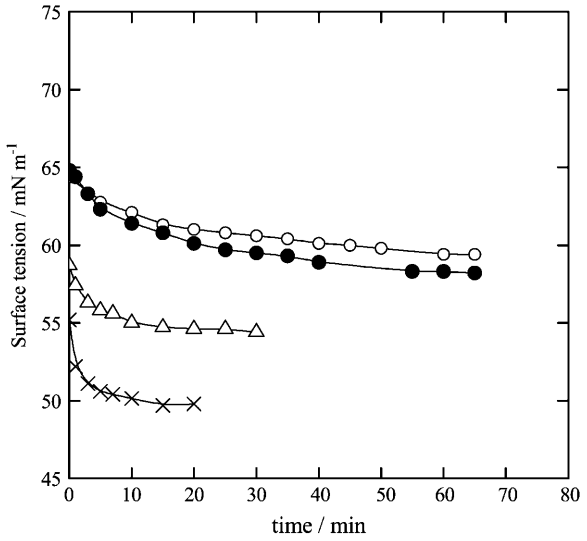

FIGURE 3 Variation of surface tension with time for aqueous solutions of foam proteins with concentrations (mg ml^{-1}): 1×10^{-3} (○), 7×10^{-3} (●), 5×10^{-2} (△), and 0.5 (×). The continuous lines are drawn to guide the eye.

surface is followed by a somewhat slower decline, the rate and extent of which depends on concentration. These slow processes may reflect the kinetics of mass transport, diffusion, or rearrangement of proteins and other macromolecules at the interface. They may also result from structural changes in the proteins, possibly including (partial) unfolding, refolding brought about by mechanical stresses in the interface, or chemical changes such as oxidation when exposed to air. All such effects are likely to contribute to the longer-term stability of protein interfacial layers and foams. It is worth noting, however, that the rates of surface tension equilibration observed here with frog foam proteins (Fig. 3) are significantly faster than observed with other proteins under similar conditions. Frog foam surface tensions stabilize in <5–10 min except at very low concentrations, but even here the equilibration was complete within 1 h. This contrasts markedly with the much longer equilibration timescales observed for other proteins such as BSA, casein, or lysozyme at similar w/v concentrations (Graham and Phillips, 1979; Damodaran and Song, 1988; Song and Damodaran, 1991; Anand and Damodaran, 1995), often involving biphasic kinetics with lag or induction phases stretching to several hours. The kinetics of surface adsorption depends greatly on charge, conformation, and chemical modification of the protein, and data in the literature even for standard proteins are not always consistent because of variations in sample preparation and experimental procedures. Graham and Phillips (1979), for example, show a slow monotonic decrease in surface tension with time (over many hours) for β-casein and lysozyme in 0.02 M phosphate buffer, pH 7, at protein concentrations of $\sim$0.7 μg ml^{-1}. However, others have reported that both surface tension and surface adsorption of lysozyme change very little over the first few hours, but that this induction period is typically followed by a rather sharp decrease of surface tension (Anand and Damodaran, 1995; Xu and Damodaran, 1994). Such biphasic kinetic behavior is also seen with other proteins. This apparent discrepancy may be caused by different experimental conditions. For example, in the work of Damodaran et al., the surface of the protein solution was always freshly swept before the surface tension measurement was started. Graham and Phillips started their tension measurement immediately after protein solution was either injected into a buffer solution or directly poured in the sample trough. And both groups used chemically modified proteins for labeling purposes (Graham and Phillips, 1979; Xu and Damodaran, 1994; Anand and Damodaran, 1995). Our tension measurements have been done using conditions similar to those adopted by Graham and Phillips, though with unmodified proteins, to represent more closely the natural situation. Long-term changes in surface tension, especially involving a lag phase, are probably more representative of chemical or conformational changes in the proteins rather than any inherent surface effects. It is probably also worth noting that lysozyme is known to undergo aggregation at the molecular level at neutral pH, and this may have some influence on its surface properties.

Regardless of the experimental uncertainties with other proteins, it is clear that the reduction in surface tension brought about by frog foam nest proteins is significantly greater and faster than so far observed with proteins from more conventional sources. It is particularly significant that we do not observe any long-term induction phase in the frog foam surfactant behavior, suggesting that gross structural or chemical changes are not required for the production of foam with ranaspumins. Of course, foam production or stabilization is not a normal biological function of any of the reference proteins used hitherto in interfacial studies, so it is perhaps not surprising that more effective systems have evolved in response to specific requirements.

Fluorescence

ANS is a fluorescent dye that binds relatively nonspecifically to hydrophobic regions on proteins (Stryer, 1965). Such binding is detectable by the increase in fluorescence emission intensity and the blue shift in emission wavelength of ANS when bound in nonpolar environments. Addition of frog foam fluid to a dilute aqueous solution of ANS (Fig. 4) gives an increase in fluorescence intensity and blue shift consistent with binding of ANS to at least some of the proteins in the mixture. The fluorescence blue shift is even greater when a small amount of ANS solution is mixed with intact foam. This indicates that at least some of the proteins present in the natural foam mixture have exposed hydrophobic regions compatible with the amphipathic nature of molecules required for surfactant activity. Moreover, the preponderance of such hydrophobic sites seems to be enhanced in the foam compared to bulk solution, presumably because much more of the protein is in the air-water interface

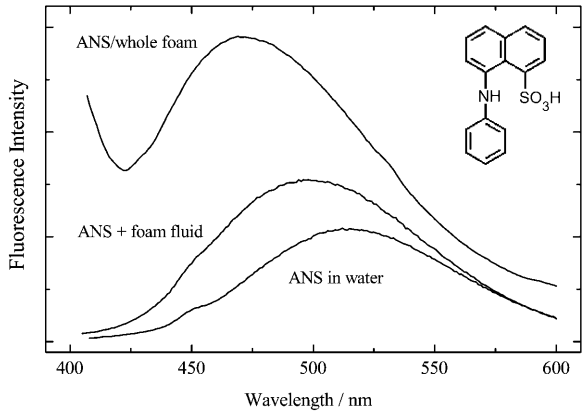

FIGURE 4 Fluorescence emission spectra of ANS ($\lambda_{exc} = 390$ nm) in nest foam and dilute foam fluid, compared to the parent spectrum in water alone. (The structure of ANS is inset.)

environment in the foam than in solution. The polarized nature of the air-water interface is most likely to promote the segregation of hydrophilic and hydrophobic portions, which would stimulate surface aggregation.

Although we have no evidence for significant aggregation of ranaspumins in solution (size exclusion chromatography; data not shown), it was thought that the possible (partial) unfolding or misfolding of proteins in the foam, together with the high β-sheet content, might indicate the presence of β-amyloid-like aggregates, as observed for many other proteins under various denaturation conditions (Dobson, 2003) and for some fungal hydrophobins (Mackay et al., 2001). However, tests for amyloid-like structures in foam fluids using standard dye-binding methods (Naiki et al., 1989; Le Vine, 1999; Klunk et al., 1999) have proved negative. Fluorescence studies using Thioflavin T gave no significant fluorescence changes in the presence of foam proteins (data not shown). Nor have we seen any increase in absorbance with Congo red. Consequently, despite the preponderance of β-sheet protein secondary structure indicated by CD, we can rule out any major involvement of amyloid-like aggregate structures in these proteins, at least in the bulk phase.

Fluorescence imaging

Imaging of foam structure at depths below the surface of the foam is difficult by conventional microscopy which, in any case, gives little information about the localization of the surfactant components of the foam fluid. Taking advantage of ANS as a convenient fluorescent probe, we have used two-photon excitation fluorescence microscopy to probe deeper into the intact foam structure. The advantage of two-photon excitation here is that the longer excitation wavelength ($\lambda_{exc} = 810$ nm) allows greater depth penetration into the foam with minimal scattering and less background since fluorescence generation is localized to the excitation volume, where instantaneous photon density is high enough to produce detectable two-photon excitation events. Illustrative examples of images obtained by this method are shown in Figs. 5 and 6. Stacking of sequential optical slices has allowed us to generate three-dimensional images of regions within the foam (not shown). For the relatively wet foam illustrated here, the structure comprises mostly spherical air bubbles with diameters in the 10–100 μm range, surrounded by foam fluid.

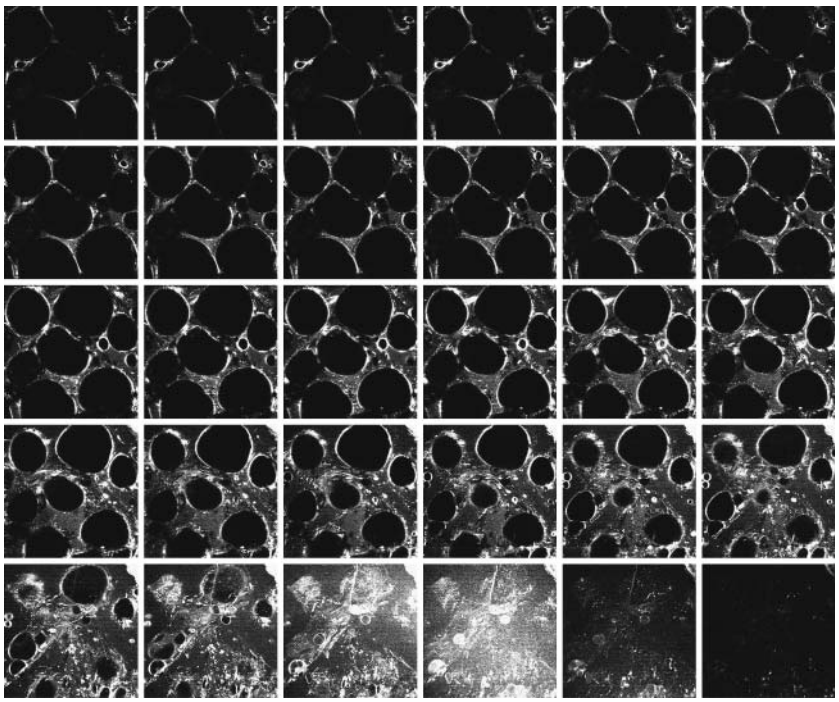

FIGURE 5 Fluorescence volume imaging of ANS-treated foam: montage of 30 planar images, in 3-μm steps, starting from point of contact with the microscope slide (*bottom right*) progressing sequentially to a total depth of ~90 μm (*top right*). Each frame is ~250 μm^2. $\lambda_{exc} = 810$ nm (200-fs pulses); $\lambda_{obs} =$ 440–500 nm, *z*-series: 3-μm slices ; 2.8-μm pixels. Trapped air bubbles appear dark in these representations.

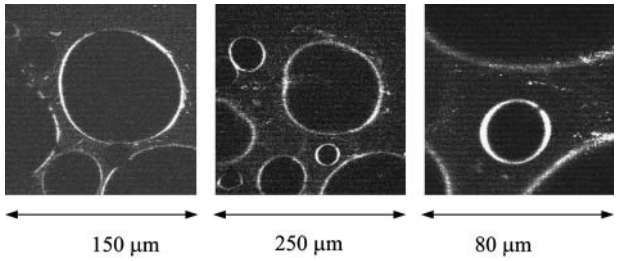

FIGURE 6 Examples of two-photon excitation microscope images of bubbles in nest foam treated with ANS. The increased fluorescence intensities show congregation of fluorescently labeled protein(s) at the air-water interface of individual bubbles within the foam.

The concentration of fluorescence intensity at the air-fluid interface of these bubbles allows their structure to be clearly resolved. This also shows that the majority of the hydrophobic probe (ANS) is concentrated at the air-fluid interface, presumably because the more hydrophobic components responsible for foam stabilization are also concentrated in this region. ANS does not have detergent-like properties, so it seems unlikely that the observed fluorescence in these images arises solely from the concentration of unbound ANS at the interface (though this is hard to prove directly since aqueous ANS solutions do not foam in the absence of protein). Nor does ANS bind to carbohydrate, so we can rule out any effect arising solely from the presence of oligosaccharides at the interface (though they may well be present in association with the proteins). Consequently, this observation of blue-shifted ANS fluorescence characteristic of the protein-bound fluorophore (Stryer, 1965) in foam images most likely reflects the anticipated congregation of proteins at the air-water interface.

These images confirm that at least some of the proteins, in particular those with a propensity to bind the hydrophobic ANS probe, and possibly together with other foam components, preferentially congregate in a layer at or near the air-water interface of entrapped bubbles. The resolution of these optical imaging techniques is insufficient to give any information regarding the structure or dimensions of this interfacial layer, but this is addressed in the next section.

Neutron reflection

Higher resolution information regarding the segregation of protein into the air-water interface has been obtained from neutron reflection experiments on frog foam proteins in solution. The reflectivity profiles were first determined at the air-NRW interface under varying protein concentrations and were found to be time-dependent in a manner consistent with that found for surface tension changes under similar conditions (Fig. 3). Since each reflectivity profile requires ~20 min for adequate neutron counting statistics, measurements were repeated consecutively at this time interval. It was found that at concentrations of 0.05 mg ml^{-1} and above, no measurable differences in reflectivity were detected after the first 2 h. At concentrations below 0.01 mg ml^{-1}, however, it was difficult to detect any change in reflectivity with time because the level of reflectivity was low. Since the surface tension measurements have indicated a longer time to reach equilibration when the protein concentration is <0.01 mg ml^{-1}, the reflectivity data were collected after the solutions were left in the troughs for ~5 h. The reflectivity profiles shown in Fig. 7 show a pronounced increase in the level of reflectivity with bulk protein concentration, indicating a strong increase of protein adsorbed as the bulk solution concentration increases. As a general rule, the steeper the curve, the thicker the protein layer. The observed increase in the slope of the reflectivity profiles with the bulk concentration indicates the increase in the thickness of the adsorbed layer.

Quantitative information about the structure and composition of the adsorbed layer can be estimated from model fitting. We have fitted all the reflectivity profiles measured in NRW using the simplest model, assuming a uniform layer distribution. The continuous lines shown in Fig. 7 are the best fits to such a model with the structural parameters given in Table 1. At the lowest concentration of 1×10^{-3} mg ml^{-1}, the data are best described by a uniform layer ~13 Å thick. However, as the total protein concentration is progressively increased, the layer thickness also increases, reaching a value of ~75 Å at the highest concentration of 0.5 mg ml^{-1}. It may appear that the final concentration increase (0.05–0.5 mg ml^{-1}) did not cause much further increase in layer thickness, hence indicating a somewhat limiting layer thickness. The situation is, however, not so straightforward. As will be described later, at the highest protein concentration

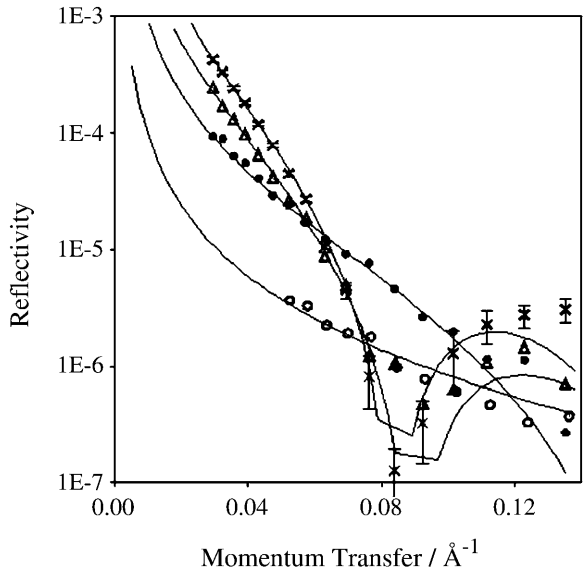

FIGURE 7 The neutron reflectivity profiles from NRW solutions with protein concentration (mg ml^{-1}) of 1×10^{-3} (○), 7×10^{-3} (●), 5×10^{-2} (△), and 0.5 (×). The continuous lines are the best fits with structural parameters listed in Table 1.

of 0.5 mg ml^{-1}, additional information from the measurement in D_2O indicates the formation of surface aggregates.

These values for surface excess (Γ) may be compared to what might be the anticipated maximum values for protein layers of such dimensions based on known volumetric properties. Partial specific volumes for proteins in aqueous solution fall in a rather narrow range ~0.72 cm^3 g^{-1} (Chalikian, 2003). Consequently, for a 75-Å layer made up entirely of protein, the surface excess would be ~10 mg m^{-2}. In reality, of course, such dense packing is not feasible, at least if the protein molecules retain their overall shape in the interface layer (packing fractions in protein crystals are typically of order 0.6). Hence Γ values of ~4–5 mg m^{-2} are not unreasonable for surface protein layers at the highest concentrations.

The dimension estimates presented so far (Table 1) were calculated assuming scattering length densities for ranaspumins equal to average values for standard proteins, since we do not yet know the distribution of the different ranaspumin components in the interface layer. Fortunately, however, the calculated parameters are relatively insensitive to this assumption, as shown in Tables 2 and 3.

In Table 2, we have listed the scattering length densities in NRW and D_2O at pH 7 for some representative globular proteins, including average values for the frog foam components based on sequence-derived amino acid compositions (R. I. Fleming, A. Cooper, and M. W. Kennedy, unpublished data), together with some typical oligosaccharides for comparison. The calculated variation with respect to D_2O content of the solvent arises from H/D exchange of labile hydrogens within the macromolecules, assuming complete exchange of labile hydrogens with bulk water. We have previously demonstrated that any incomplete exchange will have little effect on the values of ρ_{NRW} and that the uncertainty in ρ_{D_2O} is largely <5% (Su et al., 1998). It is interesting to see from Table 2 that all the ρ_{NRW} values for different proteins are very similar (within 2×10^{-7} $Å^{-2}$) and that the differences in ρ_{D_2O} do not exceed 7×10^{-7} $Å^{-2}$. The calculated scattering length densities for common oligosaccharides also fall into the same range. This observation suggests that, despite the differences in biological origin and function, as well as size and stability, the scattering length densities for these macromolecules are remarkably close. Consequently, although we do not know the entire protein/carbohydrate composition of the natural foam mixture, nor how the different components might partition differently into the interface, it is nonetheless reasonable to take the average ρ of model proteins listed in Table 2 as the mean values for the frog foam protein under appropriate isotopic contrasts. The surface excesses listed in Table 3 for frog protein were thus calculated by taking the mean value of ρ_{NRW} equal to 1.95×10^{-6} $Å^{-2}$ and that of ρ_{D_2O} equal to 3.07×10^{-6} $Å^{-2}$. These surface excesses are then compared with those obtained by using ρ values of respective reference proteins (Tables 1 and 3). It is clear that the difference between these estimates of surface excesses arising from variations in protein scattering length densities are below the level of experimental errors. Possibly more problematic would be where there is a significant amount of nonprotein material (e.g., carbohydrate) incorporated in the interface layers. Although we have some indirect evidence that this might be the case (see below), we do not yet have sufficient information to include this in the models for fitting NR data. However, in view of the anticipated similarities in scattering length densities for proteins and oligosaccharides (Table 2) this uncertainty is unlikely to affect the estimates of interface layer dimensions. What is less certain is the extent to which each layer comprises protein, carbohydrate, or a mixture of the two. For simplicity, and since we have direct evidence from fluorescence imaging of the presence of protein in the interfacial layers, we shall assume they are predominantly protein layers for the time being.

TABLE 2 Comparison of calculated scattering length densities of proteins and oligosaccharides

Protein	$\rho_{NRW} \times 10^6/Å^{-2}$	$\rho_{D_2O} \times 10^6/Å^{-2}$
β-casein	1.91	2.95
BSA	2.01	3.25
Lysozyme	2.17	3.65
Ranaspumins*	1.95 (± 0.11)	3.07 (± 0.17)
Chitin	1.99	3.38
Starch	1.83	3.57

*Mean and SD calculated from amino acid compositions of the six major protein foam components sequenced to date (Rsn-1 to Rsn-6, range for $\rho_{NRW} \times 10^6$ $Å^{-2}$ = 1.82–2.08).

TABLE 3 Surface excess calculated using different values of scattering length density

Concentration/ mg ml^{-1}	Γ_{Rsn} ± 0.3/ mg m^{-2}	Γ_{Lyz} ± 0.3/ mg m^{-2}	Γ_{BSA} ± 0.3/ mg m^{-2}	$\Gamma_{\beta\text{-CN}}$ ± 0.3/ mg m^{-2}
1×10^{-3}	0.56	0.52	0.54	0.56
7×10^{-3}	1.7	1.6	1.7	1.7
5×10^{-2}	3.0	2.8	2.9	3.0
0.5	4.4	4.0	4.2	4.3

The surface excess and layer thickness can alternatively be obtained using a more direct approach based on a kinematic approximation. Equations 1–3 show that neutron reflectivity can be directly related to the structural parameters of the layer in a simple analytical form. In the case of adsorption of a uniform layer on the surface of NRW, the relationship can be described as

$$h_{pp} = R\kappa^4/16\pi^2 b_b^2 = (4/\tau^2 A^2)\,\sin^2(\kappa\tau/2), \qquad (6)$$

where h_{pp} is the partial structure factor for the protein and A is the area per molecule and is inversely proportional to Γ. We have previously explained (Lu et al., 2000) that the dependence of reflectivity on Γ and τ can be tested by varying the two parameters independently. It is straightforward to find

that increase in Γ increases the level of reflectivity, whereas increase in τ leads to an increase in the decay of the reflectivity with κ. Thus, the two variables in Eq. 6 have different effects on reflectivity, which makes it possible to determine the two variables by fitting the single reflectivity profile. Comparison of experimental partial structure factors converted from the data shown in Fig. 7 with those of the best fits using Eq. 6 is shown in Fig. 8. The thickness and surface excess found by this method were identical with those obtained from the optical matrix treatment. It should be noted that the use of Eq. 6 requires the value of b_p for frog protein, which is unknown; we have taken this value to be equal to that of lysozyme for the purposes of this estimation.

Parallel neutron reflectivity profiles were also measured from protein mixtures in pure D_2O and the resultant profiles are shown in Fig. 9. Under this isotopic contrast, both the adsorbed protein layer and the water contribute to the reflectivity. The measurements hence offer information about the relative location of the interface layer with respect to the underlying (heavy) water. The question that can be directly addressed is the extent to which the layer protrudes from water. A further advantage of the use of pure D_2O is that the mixing of D_2O with protein helps to highlight the local inhomogeneity along the axis perpendicular to the plane of the surface. For example, if a diffuse protein layer with low volume fraction were distributed into the bulk solution underneath the main protein layer, it is difficult to identify it under NRW because the signal contribution from the diffuse layer is relatively very weak. However, the mixing of such a diffuse layer into D_2O will reduce the scattering length density over the region, which makes the D_2O measurement far more accurate.

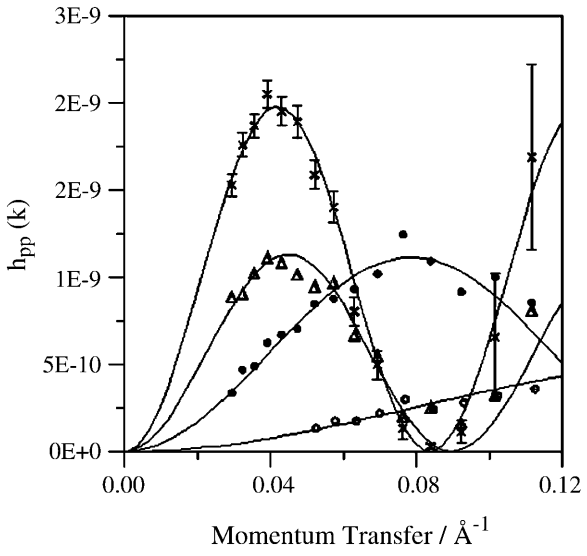

FIGURE 8 Plots of protein partial structure factors versus momentum transfer (κ) at bulk protein concentrations (mg ml^{-1}) of 1×10^{-3} (○), 7×10^{-3} (●), 5×10^{-2} (△), and 0.5 (×). The continuous lines are the best fits calculated using a single uniform layer model with structural parameters given in Table 1.

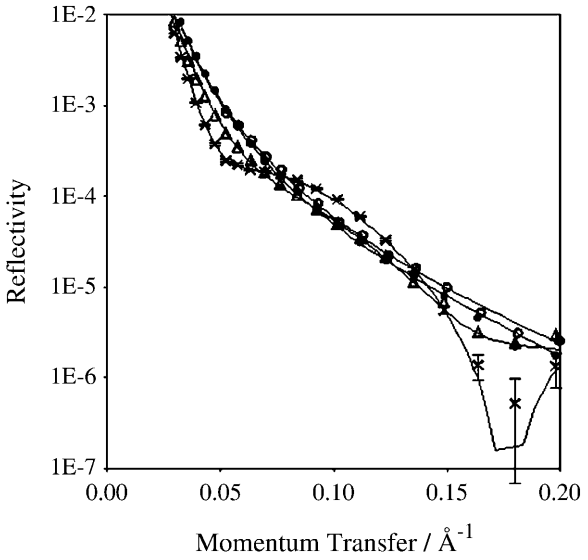

FIGURE 9 Neutron reflectivity profiles measured in D_2O solutions with bulk protein concentrations (mg ml^{-1}) of 1×10^{-3} (○), 7×10^{-3} (●), 5×10^{-2} (△), and 0.5 (×). The continuous lines represent the best fits using multilayer models and structural parameters listed in Table 4.

For all the four protein concentrations, a uniform layer model was found to be inappropriate in D_2O and two- or three-layer models were required (Table 4). This immediately rules out the possibility that the whole layer be completely immersed in or fully protruding from the solvent water. If the layer is partly immersed, then a two-layer model is required, because the additional signal from D_2O in the immersed part of the layer makes its scattering length density much greater than the corresponding value in the protruding layer. Hence, the dividing plane for the two-layer model is the surface of water. For the three low concentrations, this model with partial immersion was found to fit the measured reflectivity profiles well. But at the highest concentration of 0.5 mg ml^{-1}, the two-layer model was no longer satisfactory, and a minimum of three layers had to be used to fit the data

TABLE 4 Structural parameters for multilayer models obtained from neutron reflection measurements in D_2O

Concentration (mg ml^{-1})	τ/Å	$\rho \times 10^6$/Å^{-2}	Γ_{total}/mg m^{-2}
1×10^{-3}	$\tau_1 = 8$	$\rho_1 = 3.0$	0.5 ± 0.2
	$\tau_2 = 6$	$\rho_2 = 6.0$	
7×10^{-3}	$\tau_1 = 10$	$\rho_1 = 2.5$	1.6 ± 0.3
	$\tau_2 = 30$	$\rho_2 = 5.9$	
5×10^{-2}	$\tau_1 = 13$	$\rho_1 = 1.0$	2.8 ± 0.3
	$\tau_2 = 57$	$\rho_2 = 5.6$	
0.5	$\tau_1 = 20$	$\rho_1 = 1.0$	4.3 ± 0.5
	$\tau_2 = 35$	$\rho_2 = 5.5$	
	$\tau_3 = 20$	$\rho_2 = 4.0$	

*The combined error in Γ is ±0.3 m gm^{-2} and that in τ is ±3 Å.

adequately. The inhomogeneity arises from the immersed part of the layer. It is obvious from Table 4 that ρ within the immersed portion varies in a rather unusual manner, marked by the fact that the scattering length density for the second layer (ρ_2) is much greater than the value for the third layer (ρ_3). Since the model has assumed the full immersion of the second and third layers in D_2O, a lower ρ_3 would imply a greater volume fraction of polypeptide fragments in the third layer than in the second layer. This result appears to be inconsistent with the uniform density distribution outlined earlier. We will discuss this again later.

Two interesting observations can be obtained from the data in Table 4. First, despite the use of two- or three-layer models, the total thickness of the protein layer at a given bulk concentration is the same as obtained from the uniform layer analysis under NRW, suggesting that apart from the determination of surface excess, the uniform layer model under NRW also offers a good estimate of the dimension of the layers. Second, the thickness of the first layer increases with the bulk protein concentration, suggesting the increase in the extent of protrusion of the layer out of water. Consistent with this is the increased extent of dryness of the layer, evidenced by the decrease of ρ_1 from 3×10^{-6} Å^{-2} at the lowest concentration to 1×10^{-6} Å^{-2} at the highest concentration. The variation of ρ indicates that when the surface concentration is low, the top layer is partially mixed with water. With the increase in surface concentration this part of the layer is pushed out of the water. At the highest concentration of 0.5 mg ml^{-1} ρ_1 is 1×10^{-6} Å^{-2} in D_2O as compared with 0.8×10^{-6} Å^{-2} in NRW. The difference is a direct result of the exchange of labile hydrogens with deuterium atoms when the layer was formed from D_2O. However, under the condition of full exchange of H and D, ρ_1 should be close to 1.3×10^{-6} Å^{-2} in D_2O to conserve the fraction of protein of 0.4. A lower ρ_1 is indicative of the preferential segregation of different protein components within the layer. Given sufficient mobility within the adsorbed layer, the different proteins might self-assemble in such a way that hydrophobic regions partition away from water, whereas more polar regions remain associated with water. Since labile hydrogens are mainly associated with the polar and charged groups and to a lesser extent with the hydrophobic regions, it is reasonable to assume that the actual ρ_p of the hydrophobic part is lower than the observed mean value of 3.28×10^{-6} Å^{-2}, whereas that of the hydrophilic part is correspondingly greater. It is also possible that H/D exchange of more compact regions of the proteins might not be complete on the timescale of these experiments. This would imply that the use of mean ρ_p in the segregated layer leads to the overestimation of the adsorbed amount in the hydrophobic region and its underestimation in the hydrophilic region.

The low values of the measured ρ_1 are consistent with the apparent high values of ρ_2. At the lowest concentration of 1×10^{-3} mg ml^{-1}, there is no information available about the possible segregation merely from ρ_1, because under this condition the top layer is partly associated with water. Nevertheless, some information about the segregation can still be found from the immersed part of the layer. According to the NRW measurement, $\phi_p = 0.3$, and this corresponds to $\rho_2 = 5.4 \times 10^{-6}$ Å^{-2} in D_2O because this part of the layer is fully immersed. But the best-fitted value of ρ_2 has a significantly higher value of 6.0×10^{-6} Å^{-2} . At first sight this would indicate only a small portion of protein was immersed into D_2O. If this were the case, however, there would be a large discrepancy in the thickness and adsorbed amount obtained between the two parallel measurements using NRW and D_2O, which is improbable. The simplest explanation is preferential segregation within the adsorbed layer. As already explained, the apparently high ρ_2 resulted from the presence of a large fraction of labile hydrogens. As the concentration increases, ϕ_p is constant but the best-fitted ρ_2 decreases, suggesting a reduced extent of segregation. At 5×10^{-2} mg ml^{-1}, the best-fitted ρ_2 in D_2O is only 0.2×10^{-6} Å^{-2} greater than the mean value of 5.4×10^{-6} Å^{-2}. This difference, though small, is again consistent with the opposite trend of change between the best-fitted ρ_1 and its corresponding mean value.

Although the results at the highest concentration support the main trend of preferential segregation observed at other concentrations, the structure is characterized by a large variation of scattering length density across the layer. Since ϕ_p is 0.4, the mean ρ_2 (or ρ_3) is 5.1×10^{-6} Å^{-2}. The best-fitted three-layer model shows that ρ_1 is 1×10^{-6} Å^{-2} as compared with the mean value of 1.3×10^{-6} Å^{-2}; ρ_2 is 5.5×10^{-6} Å^{-2} and ρ_3 is 4.1×10^{-6} Å^{-2} as compared with the mean value of 5.1×10^{-6} Å^{-2}. This layered structure tends to indicate the formation of surface aggregates. The lower values of the best-fitted ρ_1 and ρ_3 suggest the adsorption of hydrophobic fragments within these regions, whereas the higher ρ_2 suggests the entrapment of relatively hydrophilic fragments. The variation of scattering length densities in the immersed part must therefore arise from the replacement of exchangeable H by D. Such exchange has little effect on ρ in NRW but drastically alters ρ in response to the distribution of polar and charged groups in D_2O. This would explain why ρ is very inhomogeneous in D_2O but uniform in NRW. In NRW, all the reflectivity profiles are adequately described by a uniform layer model. This result clearly shows that at each concentration the scattering length density is approximately uniform. This can only be true if the scattering length densities are numerically similar for the different proteins within the layer, and for the different hydrophobic and hydrophilic regions within each of these proteins. This is because NRW only contains 8% D_2O, and differential H/D exchange will make only minor differences. In D_2O, the exchange of labile hydrogens alters the scattering length density of the whole protein molecule. If no preferential segregation occurs, the scattering length density for the top layer should only be affected by the exchange of labile hydrogens and that for the

immersed layer contains an additional contribution from the presence of D_2O. The deviation of scattering length densities from their mean values calculated from the uniform layer distribution is then indicative of the extent of the preferential distributions of the hydrophilic and hydrophobic fragments. At the three low concentrations, the layers above water contain more hydrophobic fragments and the layers under water contain more hydrophilic polar and charged groups, as indicated by the deviations of ρ_1 and ρ_2 from their corresponding mean values. The structural distribution at the highest concentration is indicative of the formation of surface aggregates. The combined results suggest that the volume fractions of the polypeptide across the layers are approximately uniform. Further work will require investigation of the relationship between the structural information of the adsorbed layers obtained in this work and the stability of the foams.

It must be borne in mind that all our measurements so far have been on the natural mixture of proteins and other components in the *P. pustulosus* foam nest. This has the advantage that we can observe the natural material complete with all its constituents, usually under conditions where it functions best. The disadvantage, however, is that we are working with a mixture of molecules, each of which may play different roles in the formation, stabilization, or other functions in the foam. The six ranaspumins whose primary structure we have established remain an incomplete inventory of the foam proteins, and we do not yet have direct structural and functional information on any of them. There are also carbohydrates (polysaccharides) in the foam fluid about which we know even less. However, by amino acid sequence comparison with known proteins we have been able to predict possible functions of some of the foam components (R. I. Fleming, A. Cooper, and M. W. Kennedy, unpublished data). Some of the protein sequences have distinctly amphipathic characteristics, with charged hydrophilic tails. Others may have carbohydrate-binding (lectin) properties. And some of these may have both properties combined. Yet others may have antimicrobial or other biological activities not directly related to foam structure, but which could be present in the natural material for other biological reasons. Given this general background, together with the biophysical measurements reported here, we might begin to envisage the possible interactions at the air-water interface of the foam. During the creation of the foam, initial bubble formation and surface tension reduction at the fresh interface may involve migration of some of the more amphiphilic proteins into the air-water interface, forming an initial (mono?)layer possibly corresponding to the surface layers seen at low protein concentrations. Subsequently, different sets of proteins might assemble into or beneath this initial layer to stabilize the structure. Some of these proteins may have carbohydrate binding properties that might allow the interface to be further stabilized by the noncovalent cross-linking of polysaccharides, held together by protein-carbohydrate interactions. The final foam structure would then have the long-term stability and ability to retain moisture required for its biological function as a protective environment for developing eggs and tadpoles.

In general, the formation and stability of liquid foams depends on a number of factors, including surface tension, viscosity, cross-linking, water retention, drainage, resistance to microbial degradation, and so forth. We have shown here how, given the appropriate biological context, protein mixtures have evolved that satisfy many of these requirements. The reduced surface tension in dilute ranaspumin mixtures allows the fluid to overcome the high surface energies usually encountered with water, permitting bubble and foam formation in a fashion similar to that seen with synthetic soaps and detergents. But such foams are, usually, relatively short-lived, and tend to collapse over periods of minutes to hours because of the inherent thermodynamic instability of foams with respect to the bulk fluid. The *P. pustulosus* foams studied here have much greater long-term stability (several days under ambient tropical conditions) and surface tension alone is insufficient to explain this stability. We have shown here from both surface tension and neutron reflection data that initial formation of the air-water interface is followed by slower processes, probably involving molecular migrations, rearrangements, or more specific self-assembly processes to reinforce the newly-formed foam structure. The models most consistent with neutron reflectivity data suggest an air-water interface layer rather thicker than might be anticipated from a simple monolayer of globular proteins of the size found for ranaspumins. Globular proteins in the 10–40 kDa range typically have dimensions of order 25–45 Å, compared to the ~75 Å layer depth derived from neutron data, and spectroscopic data (CD and fluorescence) suggest that, at least in bulk solution, the conformations of ranaspumins are folded and compact. So, unless major conformational disruption occurs for proteins at the interface, the final surface structure probably comprises several layers involving a mixture of proteins, possibly also recruiting long-chain carbohydrates in the mixture to form an underlying cross-linked matrix of macromolecular interactions that would provide both the mechanical stability and water of hydration retention required to suppress drainage and subsequent collapse of the foam.

Much of this is pure speculation at this stage. But it does provide the framework for testable models. The next stage of our investigation focuses on the structure and properties of the individual protein components, and their individual roles in the surface association and organization of nest macromolecules at the air-liquid interface.

SUPPLEMENTARY MATERIAL

An online supplement to this article can be found by visiting BJ Online at http://www.biophysj.org.

We are grateful to Roger Downie, the late Peter Bacon, Margaret Nutley, Sharon Kelly (CD), Ann Dell and colleagues (carbohydrate analysis), Les Fixter (lipid analysis), and David Boodoo and the Trinidad Wildlife Service for their enthusiasm, advice, assistance, and access to facilities.

This work was supported by the Wellcome Trust Showcase scheme, the United Kingdom Biotechnology and Biological Sciences Research Council, and the Carnegie Trust for the Universities of Scotland (A.C. and M.W.K., Glasgow) and the United Kingdom Engineering and Physical Sciences Research Council (J.L., University of Manchester Institute of Science and Technology).

REFERENCES

Adamson, A. W., and A. P. Gast. 1997. Physical Chemistry of Surfaces. John Wiley & Sons, New York.

Anand, K., and S. Damodaran. 1995. Kinetics of adsorption of lysozyme and bovine serum albumin at the air-water interface from a binary mixture. *J. Colloid Interface Sci.* 176:63–73.

Bradford, M. 1976. A rapid and sensitive method for the quantitation of microgram quantities of protein utilizing the principle of protein-dye binding. *Anal. Biochem.* 72:248–254.

Chalikian, T. V. 2003. Volumetric properties of proteins. *Annu. Rev. Biophys. Biomol. Struct.* 32:207–235.

Clarkson, J. R., Z. F. Chui, and R. C. Darton. 1999. Protein denaturation in foam. II. Surface activity and conformational change. *J. Colloid Interface Sci.* 215:333–338.

Damodaran, S., and K. B. Song. 1988. Kinetics of adsorption of proteins at interfaces: role of protein conformation in diffusional adsorption. *Biochim. Biophys. Acta.* 954:253–264.

Dixon, A., G. Hogg, and N. Louahab. 2001. Design optimization of a commercial multi-photon laser scanning microscope system. *Proc. of SPIE Conf.* 4262:62–71.

Dobson, C. M. 2003. Protein folding and misfolding. *Nature*. 426:884–890.

Downie, J. R. 1988. Functions of the foam in the foam-nesting leptodactylid physalaemus-pustulosus. *Herpetol. J.* 1:302–307.

Downie, J. R. 1990. Functions of the foam in foam-nesting leptodactylids: antipredator effects of *Physalaemus pustulosus* foam. *Herpetol. J.* 1: 501–503.

Downie, J. R. 1993. Functions of the foam in foam-nesting leptodactylids: the nest as a post-hatching refuge in *Physalaemus pustulosus*. *Herpetol. J.* 3:35–42.

Dubois, M., K. A. Gilles, J. K. Hamilton, P. A. Rebers, and F. Smith. 1956. Colorimetric method for determination of sugars and related substances. *Anal. Chem.* 28:350–356.

du Noüy, P. L. 1922a. Spontaneous decrease of the surface tension of serum.: I. *J. Exp. Med.* 35:575–597.

du Noüy, P. L. 1922b. Surface tension of serum. II. Action of time on the surface tension of serum solutions. *J. Exp. Med.* 35:707–735.

Graham, D. E., and M. C. Phillips. 1979. Proteins at liquid interfaces 1. Kinetics of adsorption and surface denaturation. *J. Colloid Interface Sci.* 70:403–414.

Green, R. J., T. J. Su, J. R. Lu, J. Webster, and J. Penfold. 2000. Competitive adsorption of lysozyme and $C_{12}E_5$ at the air/liquid interface. *Phys. Chem. Chem. Phys.* 2:5222–5229.

Hakanpää, J., A. Paananen, S. Askolin, T. Nakari-Setälä, T. Parkkinen, M. Penttilä, M. B. Linder, and J. Rouvinen. 2004. Atomic resolution structure of the HFBII hydrophobin, a self-assembling amphiphile. *J. Biol. Chem.* 279:534–539.

Klunk, W. E., R. F. Jacob, and R. P. Mason. 1999. Quantifying amyloid by congo red spectral shift assay. *Methods Enzymol.* 309:285–305.

Le Vine, H. 1999. Quantification of β-sheet amyloid fibril structures with thioflavin T. *Methods Enzymol.* 309:274–284.

Lu, J. R., S. Perumal, E. T. Powers, J. W. Kelly, J. R. P. Webster, and J. Penfold. 2003. Adsorption of β-hairpin peptides on the surface of water: a neutron reflection study. *J. Am. Chem. Soc.* 125:3751–3757.

Lu, J. R., T. J. Su, R. K. Thomas, J. Penfold, and J. Webster. 1998. Structural conformation of lysozyme layers at the air/water interface studied by neutron reflection. *J. Chem. Soc. Faraday Trans.* 94:3279–3287.

Lu, J. R. and R. K. Thomas. 1998. Neutron reflection from wet interfaces. *J. Chem. Soc. Faraday Trans.* 94:995–1018.

Lu, J. R., R. K. Thomas, and J. Penfold. 2000. Surfactant layers at the air/water interface: structure and composition. *Adv. Colloid Interface Sci.* 84:143–304.

Mackay, J. P., J. M. Matthews, R. D. Winefield, L. G. Mackay, R. G. Haverkamp, and M. D. Templeton. 2001. The hydrophobin EAS is largely unstructured in solution and functions by forming amyloid-like structures. *Structure*. 9:83–91.

Mackie, A. R., A. P. Gunning, P. J. Wilde, and V. J. Morris. 1999. Orogenic displacement of protein from the air/water interface by competitive adsorption. *J. Colloid Interface Sci.* 210:157–166.

McClellan, S. J., and E. I. Franses. 2003. Effect of concentration and denaturation on adsorption and surface tension of bovine serum albumin. *Colloids Surf. B.* 28:63–75.

Naiki, H., K. Higuchi, M. Hosokawa, and T. Takeda. 1989. Fluorometric determination of amyloid fibrils in vitro using the fluorescent dye, thioflavin T1. *Anal. Biochem.* 177:244–249.

Powrie, W. 1973. Chemistry of eggs and egg products. *In* Egg Science and Technology. W. Stadelman and O. Cotterill, editors. AVI Publishing, Westport, CT. 61–90.

Provencher, S. W., and J. Glöckner. 1981. Estimation of globular protein secondary structure from circular dichroism. *Biochemistry*. 20:33–37.

Song, K. B., and S. Damodaran. 1991. Influence of electrostatic forces on the adsorption of succinylated β-lactoglobulin at the air-water interface. *Langmuir*. 7:2737–2742.

Sreerama, N., and R. W. Woody. 1993. A self-consistent method for the analysis of protein secondary structure from circular dichroism. *Anal. Biochem.* 209:32–44.

Stryer, L. 1965. The interaction of a naphthalene dye with apomyoglobin and apohemoglobin. A fluorescent probe of non-polar binding sites. *J. Mol. Biol.* 13:482–495.

Su, T. J., J. R. Lu, R. K. Thomas, Z. F. Cui, and J. Penfold. 1998. The conformational structure of bovine serum albumin layers adsorbed at the silica-water interface. *J. Phys. Chem. B.* 102:8100–8108.

van der Vegt, W., H. C. van der Mei, H. A. B. Wösten, J. G. H. Wessels, and H. J. Busscher. 1996. A comparison of the surface activity of the fungal hydrophobin SC3p with those of other proteins. *Biophys. Chem.* 57:253–260.

van Koningsveld, G. A., P. Walstra, H. Gruppen, G. Wijngaards, M. A. J. S. van Boekel, and A. G. J. Voragen. 2002. Formation and stability of foam made with various potato protein preparations. *J. Agric. Food Chem.* 50:7651–7659.

Weaire, D. L., and S. Hutzler. 1999. The Physics of Foams. Oxford University Press, Oxford, UK.

Wokosin, D. L., C. M. Loughrey, and G. L. Smith. 2004. Characterization of a range of fura dyes with two-photon excitation. *Biophys. J.* 86:1726–1738.

Wösten, H. A. B., and M. L. de Vocht. 2000. Hydrophobins, the fungal coat unravelled. *Biochim. Biophys. Acta.* 1469:79–86.

Xu, S., and S. Damodaran. 1994. Kinetics of adsorption of proteins at the air-water interface from a binary mixture. *Langmuir*. 10:472–480.

Zipfel, W. R., R. M. Williams, and W. W. Webb. 2003. Nonlinear magic: multiphoton microscopy in the biosciences. *Nat. Biotechnol.* 21:1369–1377.